Practical implementation of laser polishing on additively manufactured metallic components

Mark W. McDonald, Wojciech S. Gora, Stuart G. Stevenson, Nick J. Weston, and Duncan P. Hand

View Online   Export Citation   CrossMark

ARTICLES YOU MAY BE INTERESTED IN

Practical implementation of laser polishing on additively manufactured metallic components

View Online   Export Citation   CrossMark

Mark W. McDonald,[1] (iD) Wojciech S. Gora,[1] Stuart G. Stevenson,[2] (iD) Nick J. Weston,[2] and Duncan P. Hand[1] (iD)

AFFILIATIONS

[1]Institute of Photonics and Quantum Sciences, School of Engineering and Physical Sciences, Heriot-Watt University, Edinburgh EH14 4AS, United Kingdom
[2]Renishaw plc., Research Park North, Riccarton, Edinburgh EH14 4AP, United Kingdom

ABSTRACT

Due to the continually increasing popularity of metal powder-based additive manufacturing as a production process in recent years, there has been growing research into improving the surface quality of the parts manufactured in this way. Laser polishing offers great potential as a finishing technique due to its flexibility and suitability for automation. However, the complexity of components that can be produced with additive manufacturing processes presents challenges in developing practical and flexible arrangements for implementing a laser polishing process. In this paper, we offer methods to manage height variations of parts using weakly focused beams, process components that are (roughly) cylindrical using rotational stages, and polishing of internal surfaces using simple optics. As an example application, we present finishing of additively manufactured cobalt chrome dental implants to a surface roughness of $0.45\,\mu$m in only 60 s using a low-cost fiber delivered diode array laser.

Key words: laser polishing, additive manufacturing, surface processing, optical system

I. INTRODUCTION

Laser polishing is a surface processing technique to improve surface finish using a high-power laser beam. Absorption of the laser energy on a localized area on the surface of a material leads to the formation of a melt pool, and the material flow due to surface tension provides a smooth finish once resolidified (Fig. 1).[1] The entire surface of components can, therefore, be processed simply by scanning the beam over the desired sections, which can be readily automated.

The focus of this paper is the laser polishing of parts produced using a selective laser melting (SLM) additive manufacturing process, built from either titanium alloy (Ti-6Al-4V) or cobalt chrome (Co-Cr). The SLM process allows complex 3D designs to be built directly from a computer aided design (CAD) drawing, minimizing lead times during production and lowering costs of unique products.[2,3] In recent work, we developed optimized parameters for the laser polishing process with these two materials to provide a high-quality surface finish at reasonable process rates.[4] Using a continuous wave (CW) fiber laser source, we showed that it is possible to reduce the surface roughness (S_a) from 1 to $3\,\mu$m

for Ti-6Al-4V and from $18\,\mu$m for Co-Cr to $0.8\,\mu$m in both cases. It has been shown that the temperature changes during laser polishing result in a high tensile residual stress on the surface; however, this can be entirely relieved using standard heat relieving processing.[1]

If instead a pulsed laser is used, e.g., 650 ns,[5,6] a better surface finish can be obtained, but only if the initial surface has low roughness[7] (e.g., a roughness of 200 nm was reduced to 70 nm), since it produces a significantly shallower melt pool than a CW laser.[5,6,8] However, as-built SLM parts typically have high initial roughness, so this pulsed laser "micropolishing" is generally not suitable in this case; also, for the applications of interest here, a final roughness of the order of $1\,\mu$m is sufficient.

The SLM process is typically used to make complex parts that are difficult to fabricate by other means. The laser polishing process must, therefore, be able to cope, for example, with (i) large variations in height across the surface area; (ii) blind and through holes, which could lead to excessive heat accumulation and hence deformation; (iii) cylindrical parts requiring continuous polishing around the circumference to prevent "stitching" of polishing areas
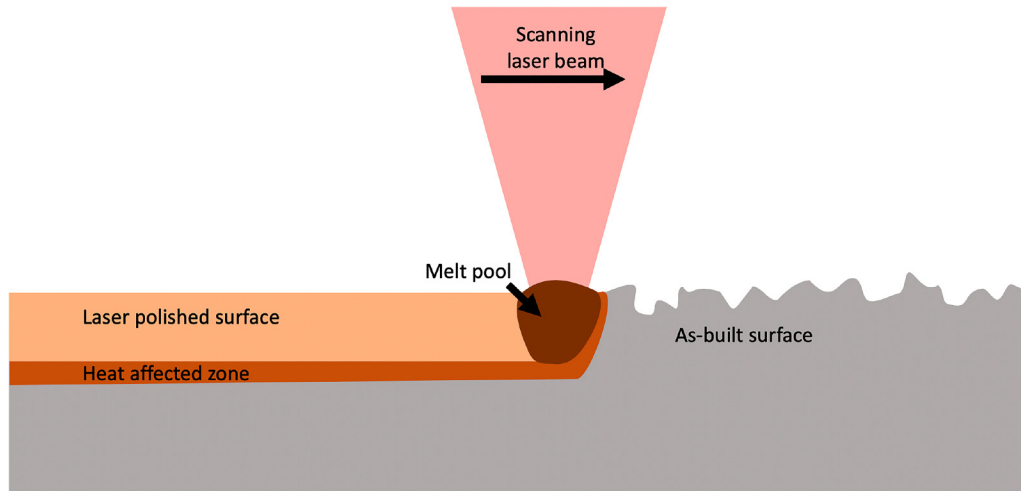
FIG. 1. Schematic diagram of the laser polishing process adapted from Ref. 1.

producing tracks; and (iv) internal channels with no direct line of sight preventing laser irradiation on the surface. These issues are not typically considered in the literature as parameter mapping is normally carried out on small planar surfaces. Morrow *et al.*[9] considered the effects of polishing on the edges of components showing that sharp edges were significantly affected by laser polishing compared to blunt or square edges that were minimally changed. Yung *et al.*[10] used a laser polishing process to improve the surface of concave and convex shapes using a layered approach in which the focal depth of the laser system and the distance of the part from focus were adjusted between each layer. This, however, requires an additional complex process control to manipulate either the workpiece or optics during laser polishing. In 2015, Flemmer *et al.*[11] reported an "industry ready" laser polishing machine capable of finishing glass moulds offering polishing rates of 40 s cm^{-2} compared with up to 5 min cm^{-2} for manual polishing while also increasing the hardness of the metal improving mould lifetime.[11,12] This is achieved by using a 5-axis machine along with a 3-axis laser scanner and complex control software to reduce incidence angles preventing elliptical beams.

In this paper, we propose and demonstrate alternative straightforward laser polishing approaches suitable for complex 3D parts. First, a telescope system is used to generate a laser spot with a long depth of focus to minimize spot size variations on the laser beam incident on the surface; second, the use of rotation stages is also demonstrated for cylindrical parts to allow for a continuous process and reduce stitching effects; and third, internal surface polishing without direct line of sight is also demonstrated using right-angled prisms.

II. SURFACE HEIGHT VARIATION

The optimization of laser polishing parameters for various materials has generally been carried out on planar surfaces,[4,5,13–18] in contrast to the actual parts produced using additive

manufacturing that are typically not flat and hence have significant height variation across the surface. Using a typical focusing lens and a scan head setup, the spot diameter (and hence the power density) of the incident beam on the surface will be strongly dependent on this height unless active focus variation compensation is introduced. Our approach to create a weakly focused beam was, therefore, to use a telescope to create a $400\,\mu$m beam waist diameter from a high beam quality (M^2 < 1.3) SPI 100W-C laser that has an emission wavelength, λ, of 1064 nm. Using a combination of two linear stages (THORLABS LTS150/M), the parts are moved under the stationary spot. A schematic of this optical layout is shown, Fig. 2, in comparison to a 2-axis galvanometer scan head and f-theta lens typically used in laser processing systems to highlight the difference in beam paths.

Using the knife edge method, $1/e^2$ beam diameter is measured over a distance of 15 cm after the telescope at a spacing of 2 cm (Fig. 3). A line has been fitted to these data to show how this beam propagates beyond this length. The theoretical beam diameter for the scan head and f-theta lens, W, as a function of propagation length, z, calculated from Eqs. (1)–(3), is also included for comparison.[19] This is based on using an f-theta lens with a focal length, f, of 160 mm and an input beam diameter, D, of 10 mm. To highlight the improved working range of the two approaches, shaded regions are included representing beam diameters of $400 \pm 100\,\mu$m,

$$W(z) = W_0^2 \sqrt{1 + \left(\frac{z}{Z_R}\right)^2}, \tag{1}$$

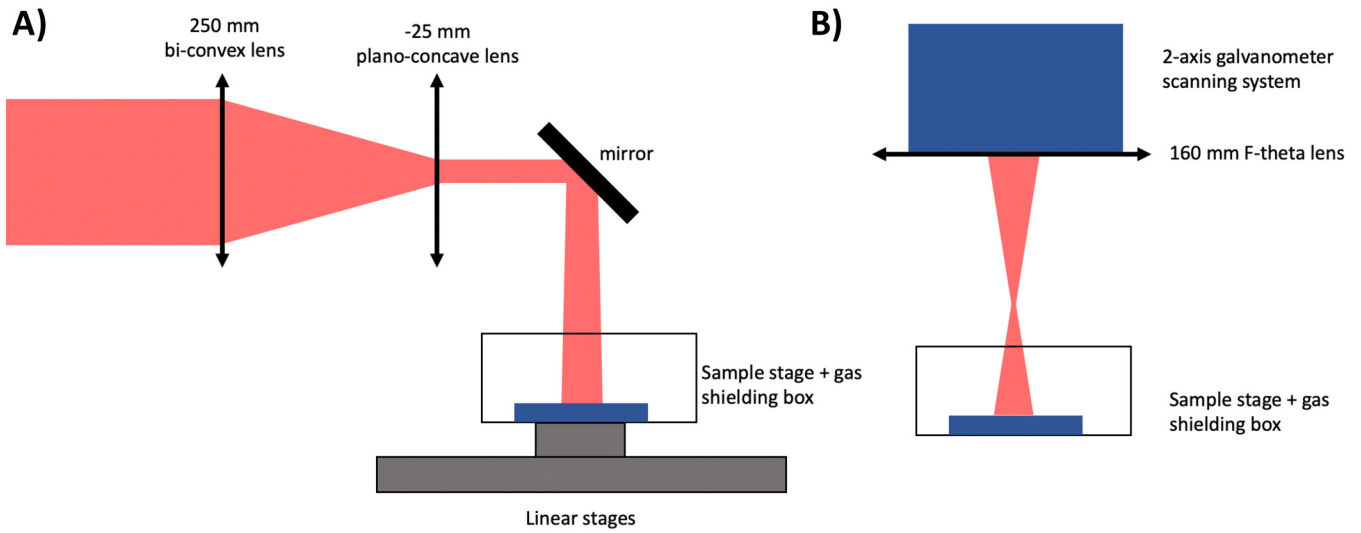$$W_0 = \frac{2\lambda F}{\pi D}, \tag{2}$$

FIG. 2. Schematics of (a) the weakly focused setup and (b) the scan head setup. Telescope constructed using a biconvex lens ($f = 250$ mm) and a planoconcave lens ($f = -25$ mm), separated by a distance of 225 mm, provides a 400 μm diameter laser spot on the surface of the material.
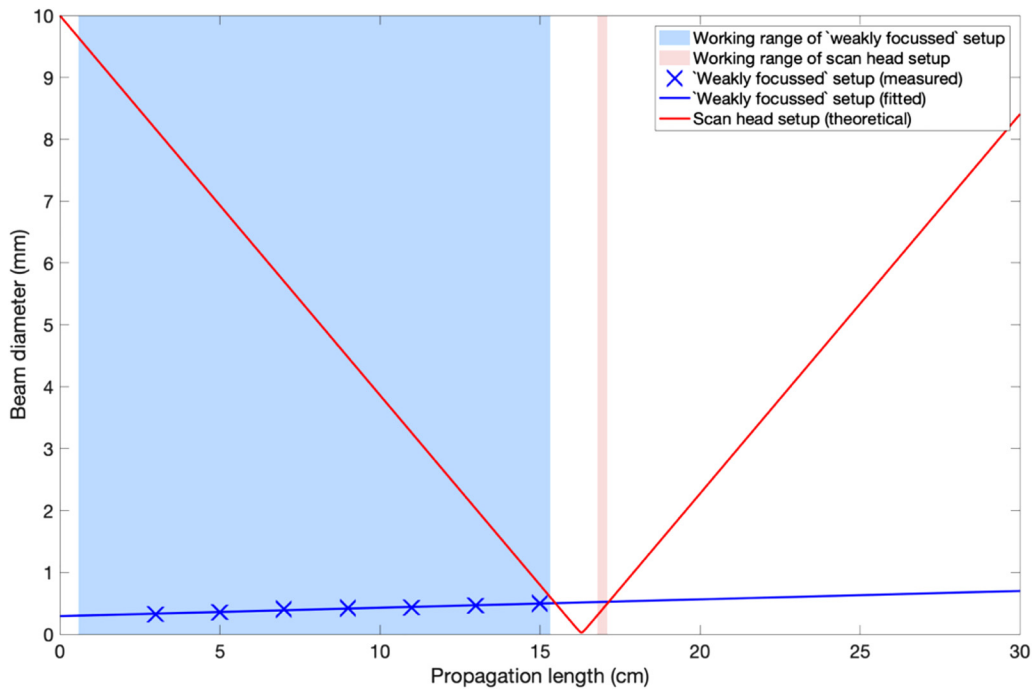
FIG. 3. Laser beam diameter as a function of distance for both the weakly focused and scan head setups. The $1/e^2$ beam diameters (blue crosses) were calculated from measurements of the 90-10 diameter using the knife edge method. A trendline (blue) is fitted to show the change of diameter with distance. The red line is the calculated beam diameter after the f-theta lens in the scan head setup. The shaded areas (blue—"weakly focused" setup; red—scan head setup) indicate the region in which the laser beam diameter is 400 $\pm$ 100 μm, as required by the polishing application.

FIG. 4. (a) Cross-sectional area and (b) the height map of a typical cranial implant. Height map is measured over the highest section of the implant.
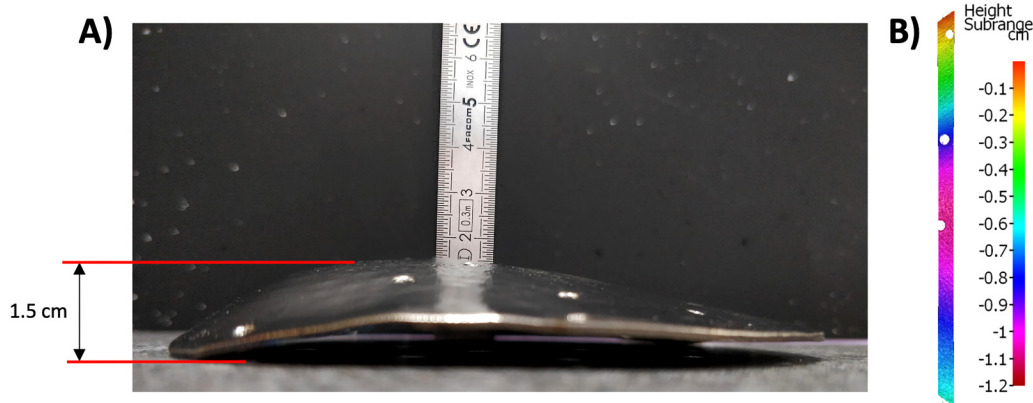
$$Z_R = \frac{\pi W_0^2}{\lambda M^2}. \tag{3}$$

A. Cranial implants

An application in which laser polishing has a significant potential benefit is in the finishing of SLM-fabricated cranial implants, which are tailored specifically to each patient using medical imaging. A major drawback to this process is the poor surface quality of the as-built parts. Due to the freeform nature and thinness (typically 1 mm) of these implants, they are currently mechanically polished using a semimanual process that adds hours of skilled work into the production line and unwanted variability. Laser polishing provides a route to process automation, improving repeatability between parts and potentially reducing costs.

The large curved shapes typical of cranial implants provide a large variation in height from the edges to the center. A typical cross section profile and height map across a section (Fig. 4) show that the implant used during testing had a height range of 1.5 cm.

The telescope approach described above allows polishing without additional focus control. To compare the performance of this approach with the scan head plus f-theta lens, a cranial implant plate was split into four quadrants, as detailed in Fig. 5: (a) weakly focused plus scan head setups, (b) weakly focused beam only, (c) scan head only, and (d) initial surface. The scanning speed of the laser beam, v, in all cases was set to 16.6 mm s^{-1}, calculated using Eq. (4) to maintain an energy density, ED, of 1.5 kJ cm^{-2} with a laser power, P, of 100 W. A hatch spacing of 280 μm was used to maintain a 30% line overlap. These parameters were taken from previously carried out optimization experiments,[4]

$$ED = \frac{P}{W \, v}. \tag{4}$$

The initial surface in this case is after an initial mechanical polished step to remove support structures produced during the build process. The resulting initial surface has a low surface roughness and waviness before laser polishing; however, there are a large number of holes across the surface. The surface height maps in each region were measured at 5× magnification (Fig. 6) using an Alicona InfiniteFocus surface profilometer. For each laser polished region, the surface height map was measured in two regions: (i) bottom, corresponding to the section of the cranial implant where the scan head setup provides a 400 μm beam diameter, and (ii) top, where the beam diameter from the scan head setup incident on the sample is smaller. No holes can be seen in the bottom region of the laser polished surfaces and are significantly reduced in number and depth in the top region.
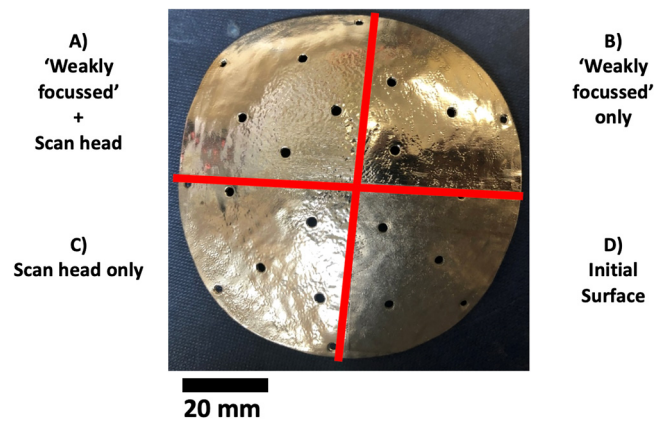

FIG. 5. Cranial implant plate that has different surface finishes in each quadrant. (a) Weakly focused and scan head setup, (b) weakly focused beam only, (c) scan head only, and (d) initial surface. The initial surface appears darker because it scatters much of the incident light due to the nature of the surface features.

ARTICLE   scitation.org/journal/jla

	Bottom region	Top region
Initial surface	A)	
Scan head	B)	C)
Scan head + Weakly Focussed	D)	E)
Weakly Focussed	F)	G)

FIG. 6. Surface profiles imaged using Alicona InfiniteFocus with 5× magnification of the cranial implant after laser polishing.

© Author(s) 2020

32, 042019-5

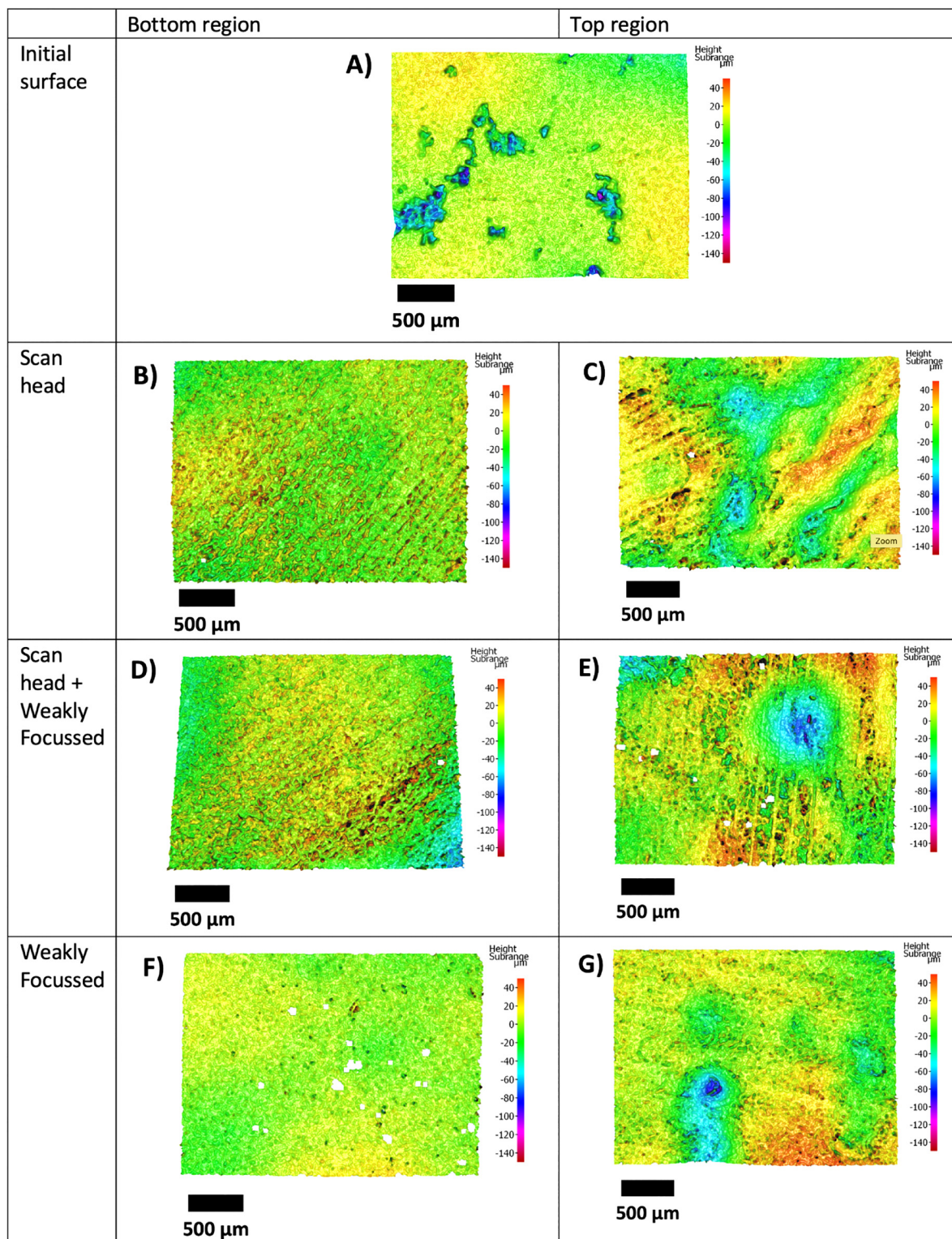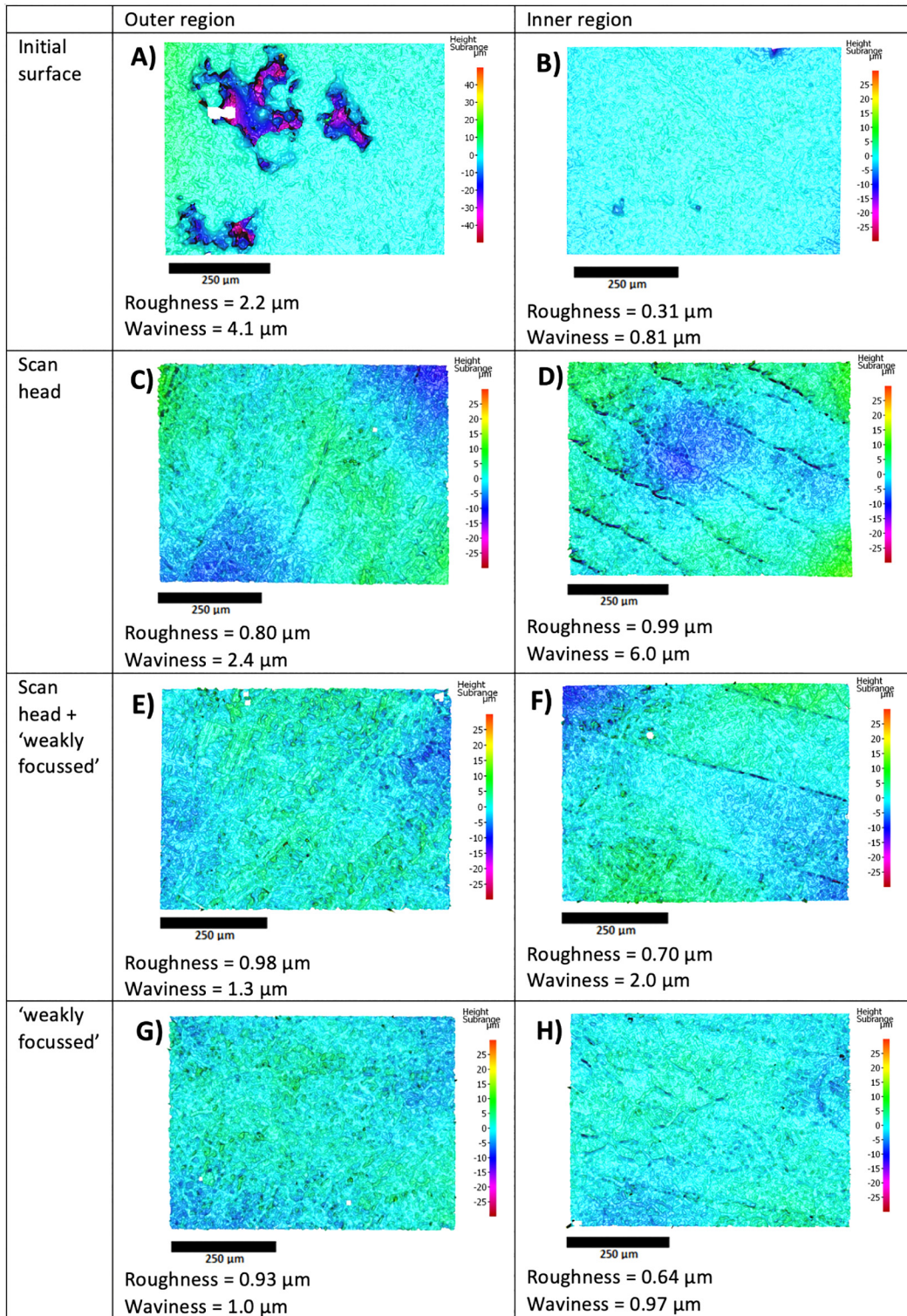**FIG. 7.** Surface profiles imaged using Alicona InfiniteFocus with 20× magnification of the cranial implant after laser polishing.
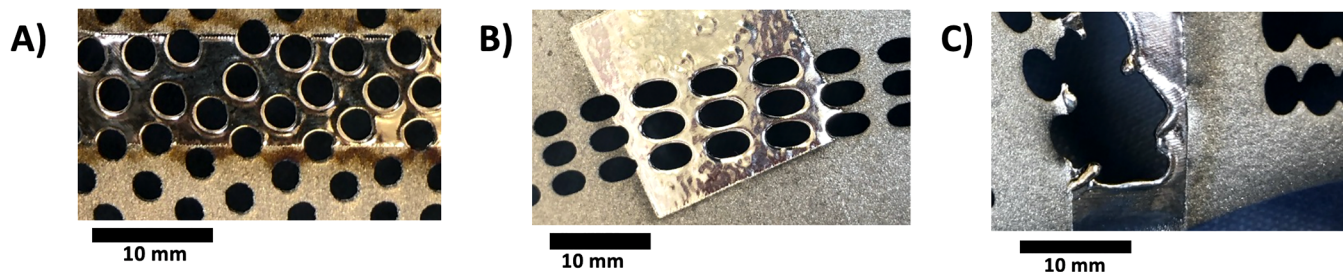
FIG. 8. Laser polishing on parts that have some surface features.

Comparing the bottom and top regions for each quadrant shows that when the scan head is used, the top regions are less smooth. This is more evident when comparing the surface roughness and waviness values at 20× magnification (Fig. 7). A similar approach was taken in which two areas were measured at the top and bottom regions in each quadrant. The roughness and waviness were calculated using a cut-off wavelength of 114 μm. The roughness in each of the laser polished regions is unchanged for both the upper and lower sections. Comparing the waviness between the top and bottom regions for each laser polished quadrant shows that the waviness increases at the top region when using the scan head setup. This is not the case when using the "weakly focused" setup, which generates a similar waviness in these two regions. The waviness is also lower when using the "weakly focused" setup compared with the scan head.

B. Surface features

Cranial implant plates also typically have some holes on the surface (in some designs these are closely spaced), which may be of concern during the laser polishing process. The energy required to melt the surface in order to polish it could also lead to excessive heating and hence deformation or even drop-outs around these holes. Examples are shown in Fig. 8, where polishing was carried out using the weakly focused beam, without altering the laser parameters in the vicinity of the holes. As stated previously, an energy density of 1.5 kJ cm^{-2} and a line overlap of 30% were used on all three parts. In the examples shown in the left and center images, the features were preserved; however, for features that come to a small point such as those in the righthand image of Fig. 8, the heat accumulation was too great and caused significant damage to the features. Using a lower energy density is likely to prevent this
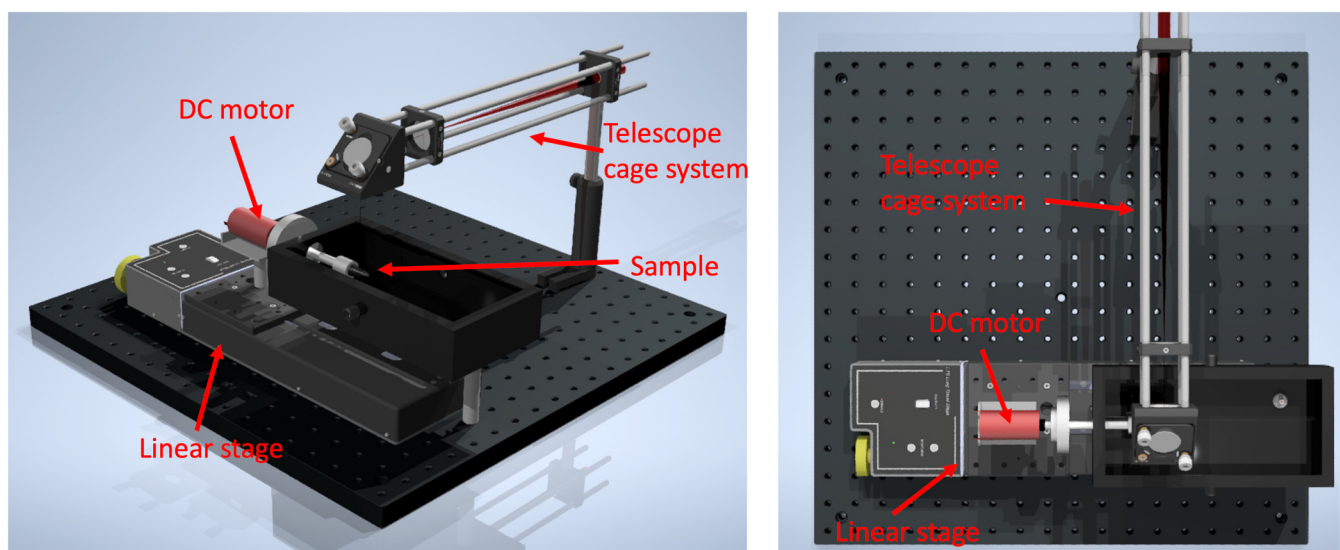

FIG. 9. 3D CAD drawing (a) and top-down view (b) of the rotation setup used to laser polish cylindrical components.

deformation. This demonstrates that while processes can be created that are relatively insensitive to the part shape, laser parameters will still have to be adapted in some cases to prevent heat accumulation. However, further investigation would be required to determine how the geometry of these features affects deformation.

III. CYLINDRICAL COMPONENTS

For parts that are cylindrical or similar and, therefore, have no edge, it is best to carry out laser polishing continuously around the whole part. This is because the polishing process produces a border, making it difficult to stitch different areas together. To accomplish this, a rotary arrangement was developed that uses a DC motor (RS Pro 413-0600) combined with a linear stage (THORLABS LTS 150/M) to rotate and move the sample under a stationary laser spot. This is controlled by a LABVIEW program to rotate the sample at the correct angular velocity in order to maintain the required energy density. The angular velocity of the stage, ω, measured in RPM is calculated from the time to travel one circumference at the linear scanning speed, v, used for flat samples using Eqs. (5) and (6). A schematic of this setup is shown in Fig. 9,

$$t = \frac{v}{\pi \mathrm{D}}, \tag{5}$$

$$\omega = \frac{60}{t}. \tag{6}$$

The line overlap is controlled using the linear stage traveling at a constant velocity that is set to have moved a distance equal to one hatch spacing in the time for one full rotation of the part. This maintains a continuous spiral along the entire length of the component.

In this case, a fiber delivered diode array laser (BWT K915FG2RN), which has a maximum power of 150 W, was investigated as an alternative, low-cost laser source (albeit low beam quality with an M^2 value of 39). A 4f optical system was implemented to produce a focal spot of $400 \, \mu m$ diameter (measured at $1/e^2$). The beam profile can be seen in Fig. 10, and it can be seen that multimode fiber delivery provides an almost top-hat shaped beam profile. This will aid the laser polishing process as it provides a more uniform temperature gradient within the melt pool compared with the Gaussian shaped beam of the fiber laser.[16] The wavelength of this diode array is 915 nm compared with 1064 nm of the fiber laser, so the absorption may be slightly different.

Dental implants are often produced using additive manufacturing techniques, given that their (roughly) cylindrical shape has the potential to be polished using the rotational stage described above. The spatial selectivity of laser polishing is beneficial in this case as dental implants require two distinct surface finishes: a rough top surface to allow bonding with the tooth crown and a smooth bottom surface to prevent irritation and bacterial growth within the mouth. The current finishing technique that is commonly used is electrochemical polishing that (as well as involving hazardous chemicals) is a nonselective process, and, hence, a second process is required to reroughen the surface to be bonded to the crown. During laser polishing tests, the top surface of the dental implants was, therefore, left in the as-built state, exploiting the spatial selectivity of the process and allowing all surface processing to be completed in one stage rather than two or more.

The size and thickness of each implant can vary depending on the tooth that is being replaced. This can affect the heat accumulation and thus the difference in laser parameters between each implant. Two variants of the implant were studied, as shown in Fig. 11. The smaller implant required a lower energy density of $2.0 \, \mathrm{kJ \, cm^{-2}}$ compared with the larger implant ($4.0 \, \mathrm{kJ \, cm^{-2}}$). As
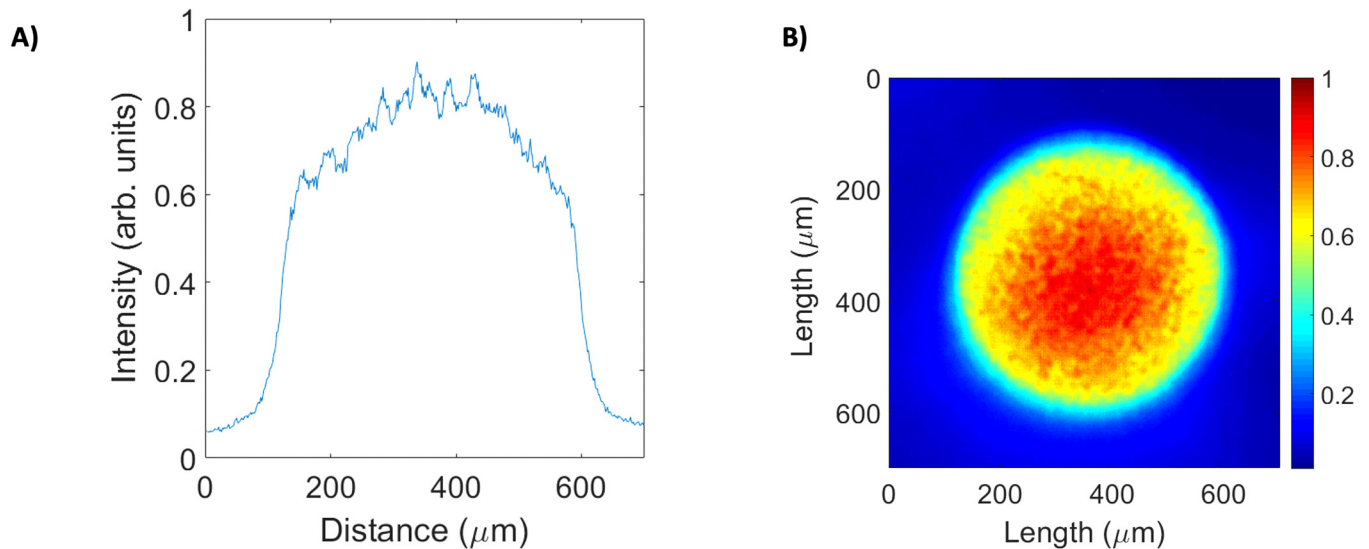
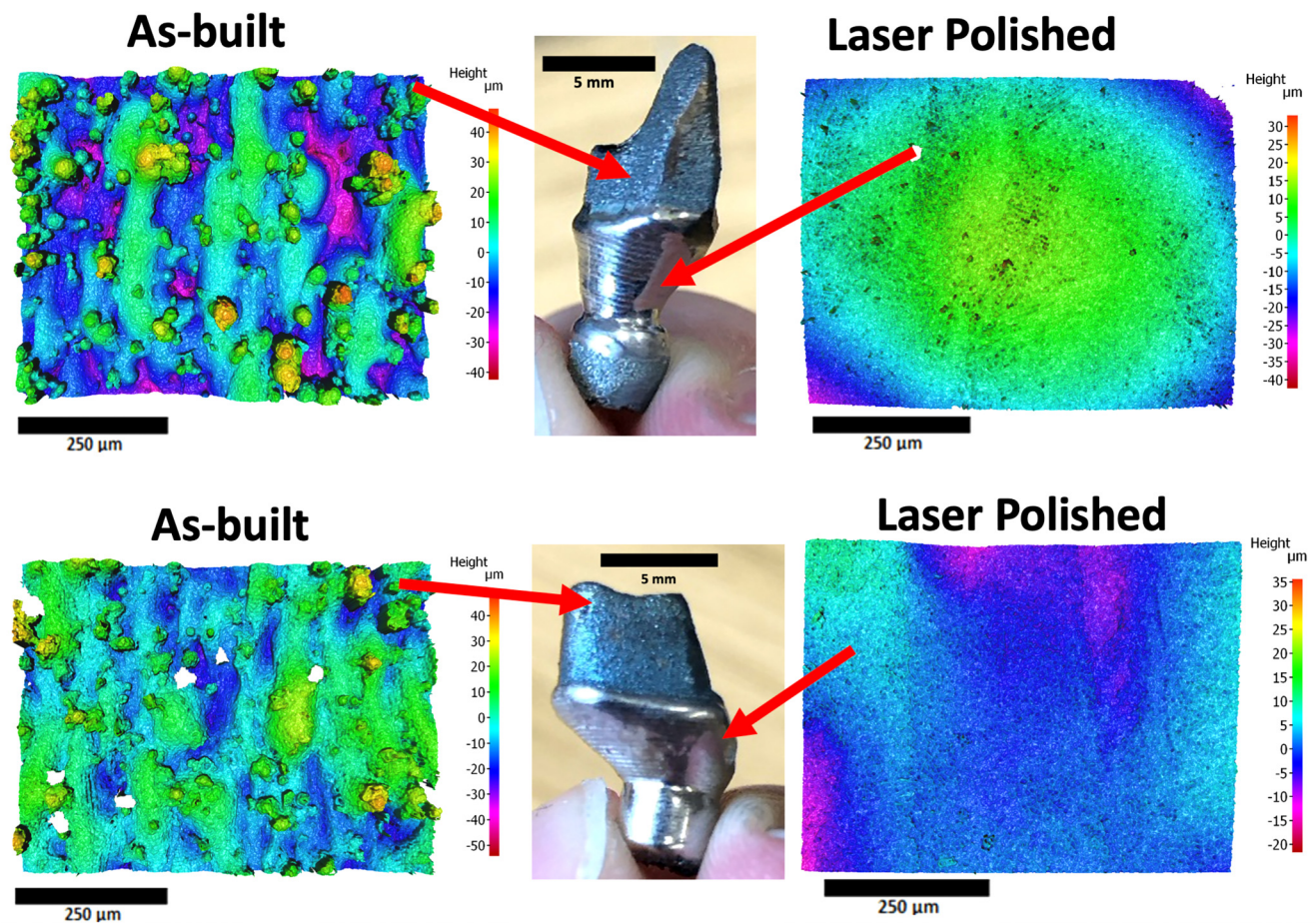**FIG. 10.** Beam profile measurements of fiber delivered diode array.

FIG. 11. 3D surface maps of small (top row) and large (bottom row) as-built and laser polished dental samples. The upper part of each sample is the original as-built surface, and only the lower area was laser polished.

with previous sections, these parameters were based on optimization experiments for cobalt chrome.[4] Some further optimization was carried out visually for the two different sized implants. This was necessary as the lower energy density was created a large enough melt with the smaller part to reduce the surface roughness. A line overlap of 50% was used in both cases. The processing time in each case was 60 and 120 s for the small and large implant, respectively. The surface profile of the implants before and after laser polishing is also shown in Fig. 11. The as-built surface roughness, Sa, was reduced from 5.6 to 0.45 μm after laser polishing for the smaller implant and 4.9 to 0.63 μm for the larger.

IV. INTERNAL CYLINDRICAL SURFACES

Additive manufacturing, due to its layer-by-layer approach, allows for straightforward creation of complex internal structures that can provide strong but lightweight structures or cooling channels. These internal surfaces, however, pose a challenge for laser polishing as there is often no direct line of sight. A possible solution to this is to reflect the light using a right-angled prism onto the surface, as shown in Fig. 12. A right-angled prism (THORLABS PS610) is mounted on a 0.5-in. lens tube attached to a rotation stage (THORLABS PRM1/MZ8). These parts were selected due to the availability as standard parts. This allows the laser light to be aligned to the center of the lens tube and the prism rotating on the lens tube provides the spot 360° of rotation around the internal surface of a 30 mm diameter cylinder. The weakly focused beam demonstrated in Sec. II is used for ease of alignment. A flow of argon inert gas was directed toward the prism to prevent oxidation of the surface. The rotation stage is set to a rotational speed of 1.26 rad s^{-1} to maintain an energy density of 1.5 kJ cm^{-2} on the internal surface that has a diameter of 27 mm. After polishing, the cylinder was sectioned to measure the internal surfaces. The photographs of the internal surface are shown in Fig. 13. The surface profiles were subsequently measured (Fig. 14), and roughness and waviness were measured to be
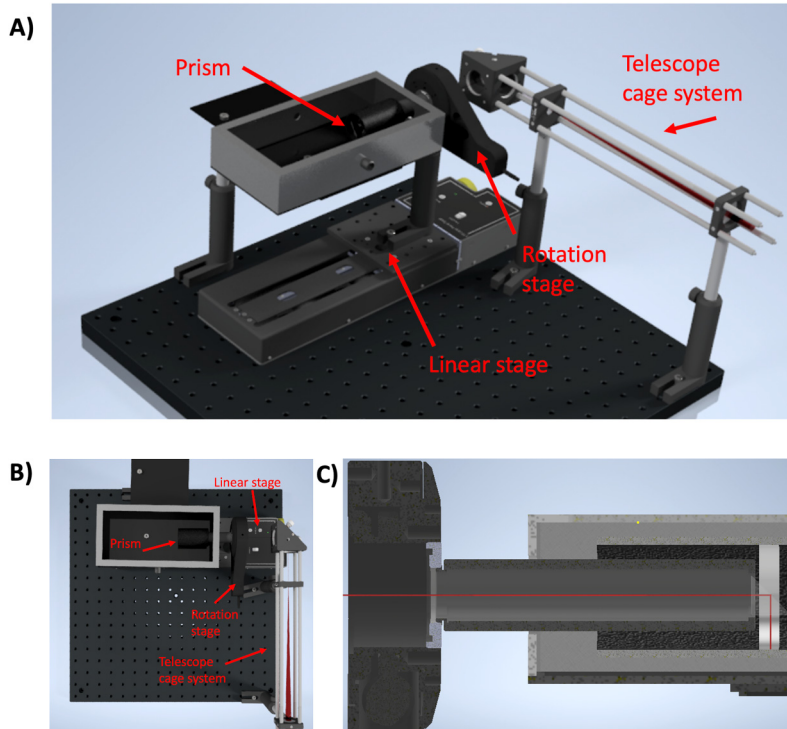
FIG. 12. 3D CAD drawing (a) and top-down view (b) of the internal laser polishing setup. Sectioned view (c) of the center of the rotation stage showing the laser beam path.

0.51 and 3.6 μm, respectively. This is an improvement from an initial roughness of 6.3 μm and a waviness of 7.2 μm. During processing, some back spatter was observed, which can damage the prism. This highlights possible limitations of the process in how close the prism can be to the processed surface. The size of the lens tube and prism that were used within this setup currently restrict the lower limit to the internal diameter of the cylinder due to the back spatter observed during processing. Implementing a smaller prism and lens tube would enable smaller cylinders to be processed; also, it is planned in future to further reduce this diameter by using an optical fiber with an angled end-face to replace the prism.
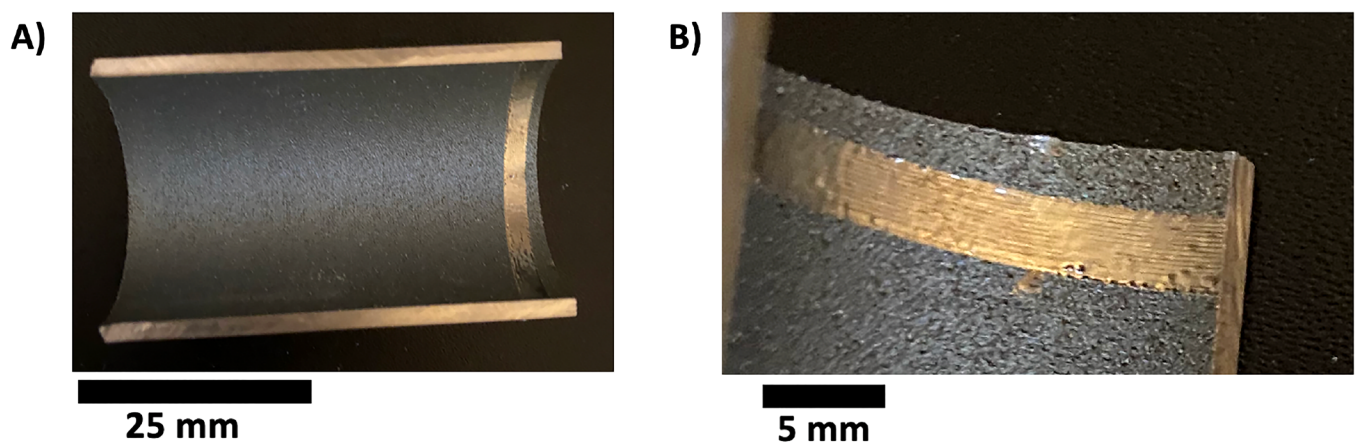

FIG. 13. Photographs of the internal surface of a hollow cylinder, which has been sectioned after polishing to view the polished area. (a) shows the full length of the cylinder and (b) shows closer to the surface.
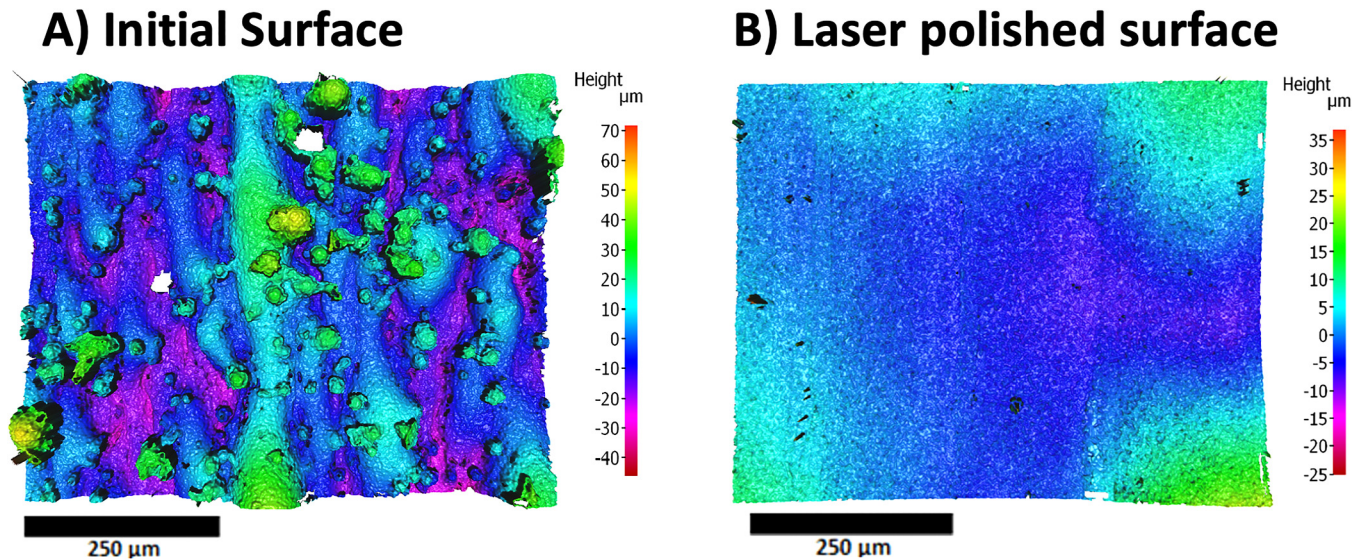
A) Initial Surface

B) Laser polished surface

FIG. 14. 3D surface maps of initial (a) and laser polished (b) surfaces.

V. CONCLUSIONS

In this paper, we have demonstrated various practical approaches to laser polishing of realistic 3D SLM-fabricated parts. The particular approach used depends on the type of part to be post-processed. For surfaces with large changes in height, a solution is to use a laser beam with minimal divergence, created by using a simple telescope. This was demonstrated with cranial implants. For parts with relatively small changes in surface height, meanwhile, it is possible to use a lower beam quality, lower cost laser system, as demonstrated with dental implants, and a rotary stage. Finally, by using a right-angled prism to redirect the laser beam, we were able to laser polish the internal surface of a hollow cylinder. This technique could be used to improve the surface quality of internal channels that previously would have been unreachable with this laser process.

ACKNOWLEDGMENTS

REFERENCES

[1]Y. Tian *et al.*, "Material interactions in laser polishing powder bed additive manufactured Ti6Al4V components," Addit. Manuf. **20**, 11–22 (2018).

[2]C. Y. Yap *et al.*, "Review of selective laser melting: Materials and applications," Appl. Phys. Rev. **2**, 041101 (2015).

[3]S. Bremen, W. Meiners, and A. Diatlov, "Selective laser melting: A manufacturing technology for the future?," Laser Tech. J. **9**, 33–38 (2012).

[4]W. S. Gora, Y. Tian, M. Ardron, P. Prangnell, N. J. Weston, and D. P. Hand, "Laser polishing to improve the surface quality of CoCr and Ti6AL4V additively manufactured parts," in *Proceedings of the 36th International Congress on Applications of Lasers and Electro-Optics (ICALEO 2017), October 22–26, 2017, Georgia, USA* (The Laser Institute of America, 2017), ISBN: 978-1-940168-14-2 p. 1045.

[5]T. L. Perry, D. Werschmoeller, X. Li, F. E. Pfefferkorn, and N. A. Duffie, "Pulsed laser polishing of micro-milled Ti6Al4V samples," J. Manuf. Process. **11**, 74–81 (2009).

[6]T. L. Perry, D. Werschmoeller, X. Li, F. E. Pfefferkorn, and N. A. Duffie, "The effect of laser pulse duration and feed rate on pulsed laser polishing of microfabricated nickel samples," J. Manuf. Sci. Eng. **131**, 031002 (2009).

[7]C. Nüsser, H. Sändker, and E. Willenborg, "Pulsed laser micro polishing of metals using dual-beam technology," Phys. Procedia **41**, 346–355 (2013).

[8]M. Vadali, C. Ma, N. A. Duffie, X. Li, and F. E. Pfefferkorn, "Effects of pulse duration on laser micro polishing," J. Micro Nano-Manuf. **1**, 291–297 (2013).

[9]J. D. Morrow, J. Vockrodt, K. Klingbeil, and F. E. Pfefferkorn, "Predicting laser polishing outcomes at edge features," J. Laser Appl. **29**, 011703 (2017).

[10]K. C. Yung, T. Y. Xiao, H. S. Choy, W. J. Wang, and Z. X. Cai, "Laser polishing of additive manufactured CoCr alloy components with complex surface geometry," J. Mater. Process. Technol. **262**, 53–64 (2018).

[11]J. Flemmer, I. Ross, E. Willenborg, and H. Fröba, "Machine tool and CAM-NC data chain for laser polishing complex shaped parts," Adv. Eng. Mater. **17**, 260–267 (2015).

[12]A. Lamikiz, J. A. Sánchez, L. N. L. de Lacalle, and J. L. Arana, "Laser polishing of parts built up by selective laser sintering," Int. J. Mach. Tools Manuf. **47**, 2040–2050 (2007).

[13]S. Marimuthu, A. Triantaphyllou, M. Antar, D. Wimpenny, H. Morton, and M. Beard, "Laser polishing of selective laser melted components," Int. J. Mach. Tools Manuf. **95**, 97–104 (2015).

[14]L. Giorleo, E. Ceretti, and C. Giardini, "Ti surface laser polishing: Effect of laser path and assist gas," Proc. CIRP **33**, 446–451 (2015).

[15]C. S. Chang, T. H. Chen, T. C. Li, S. L. Lin, S. H. Liu, and J. F. Lin, "Influence of laser beam fluence on surface quality, microstructure, mechanical properties, and tribological results for laser polishing of SKD61 tool steel," J. Mater. Process. Technol. **229**, 22–35 (2016).

[16]C. Nüsser, I. Wehrmann, and E. Willenborg, "Influence of intensity distribution and pulse duration on laser micro polishing," Phys. Procedia **12**, 462–471 (2011).

[17]C. P. Ma, Y. C. Guan, and W. Zhou, "Laser polishing of additive manufactured Ti alloys," Opt. Lasers Eng. **93**, 171–177 (2017).

[18]J. Kumstel and B. Kirsch, "Polishing titanium- and nickel-based alloys using cw-laser radiation," Phys. Procedia **41**, 362–371 (2013).

[19]E. Hecht, *Optics*, 4th ed. (Pearson, England, 2013).